A family of hyperpolarization-activated channels selective for protons

Lea Wobig[a], Thérèse Wolfenstetter[a], Sylvia Fechner[a,1], Wolfgang Bönigk[a], Heinz G. Körschen[a], Jan F. Jikeli[a], Christian Trötschel[b], Regina Feederle[c], U. Benjamin Kaupp[a,d,2,3], Reinhard Seifert[a,2,3], and Thomas K. Berger[a,e,2,3]

[a]Department of Molecular Sensory Systems, Research Center Caesar, 53175 Bonn, Germany; [b]Department of Plant Biochemistry, Ruhr-University Bochum, 44801 Bochum, Germany; [c]Monoclonal Antibody Core Facility and Research Group, Institute for Diabetes and Obesity, Helmholtz Zentrum München, German Research Center for Environmental Health, 85764 Neuherberg, Germany; [d]Life & Medical Sciences Institute (LIMES), University of Bonn, 53115 Bonn, Germany; and [e]Department of Neurophysiology, Institute of Physiology and Pathophysiology, Philipps-University Marburg, 35037 Marburg, Germany

Edited by Ehud Y. Isacoff, University of California, Berkeley, CA, and approved April 10, 2020 (received for review January 25, 2020)

Proton (H^+) channels are special: They select protons against other ions that are up to a millionfold more abundant. Only a few proton channels have been identified so far. Here, we identify a family of voltage-gated "pacemaker" channels, HCNL1, that are exquisitely selective for protons. HCNL1 activates during hyperpolarization and conducts protons into the cytosol. Surprisingly, protons permeate through the channel's voltage-sensing domain, whereas the pore domain is nonfunctional. Key to proton permeation is a methionine residue that interrupts the series of regularly spaced arginine residues in the S4 voltage sensor. HCNL1 forms a tetramer and thus contains four proton pores. Unlike classic HCN channels, HCNL1 is not gated by cyclic nucleotides. The channel is present in zebrafish sperm and carries a proton inward current that acidifies the cytosol. Our results suggest that protons rather than cyclic nucleotides serve as cellular messengers in zebrafish sperm. Through small modifications in two key functional domains, HCNL1 evolutionarily adapted to a low-Na^+ freshwater environment to conserve sperm's ability to depolarize.

HCNL1 channel | proton channel | voltage-sensing domain | HCN channel

Ion channels control the flux of ions across cell membranes, which is essential for chemical and electrical signaling. Hyperpolarization-activated and cyclic nucleotide-gated (HCN) channels belong to the superfamily of voltage-gated ion channels (1–3). On hyperpolarization, HCN channels open and carry a Na^+ inward current that in turn depolarizes the cell. They are modulated by cyclic nucleotides, and thereby, couple second-messenger signaling to electric activity (4). HCN channels, also known as pacemaker channels, serve diverse functions. They control cardiac rhythmicity (4, 5) and electrical oscillations in the vertebrate brain (6). For example, HCN channels in dendrites of many neurons shape synaptic integration (6, 7). In vertebrate retinal photoreceptors, HCN channels curtail the hyperpolarizing response to bright light and promote recovery from stimulation (8, 9). In sea urchin sperm, HCN channels participate in the signaling pathway that controls the flagellar beat during sperm chemotaxis (10, 11).

HCN channel subunits consist of six transmembrane segments (S1 to S6) and a C-terminal cytosolic cyclic nucleotide-binding domain (CNBD). Segments S1 to S4 form the voltage-sensing domain (VSD). The S4 segment serves as a voltage sensor; it carries positively charged amino acid residues, mostly arginine, at every third position. Upon hyperpolarization, the motion of S4 opens a gate near the intracellular side of the pore. Segments S5 and S6 constitute the pore domain (PD) that forms a central ion permeation pathway in the tetrameric channels; HCN channels are slightly more selective for K^+ over Na^+ but at physiological conditions carry inward Na^+ currents (1–3). Cyclic nucleotides bind to the CNBD and modulate the voltage dependence of activation.

Here, we report on a HCN channel from zebrafish sperm, named HCNL1 (for HCN-like 1). Although highly homologous to classic HCN channels, HCNL1 features two modifications that result in a completely new function. We show that HCNL1 channels carry protons with exceptional selectivity via an ion permeation pathway in the voltage sensor, whereas the pore domain is nonconducting. HCNL1 activates during hyperpolarization and acidifies the sperm cytosol. Our results suggest that HCNL1 represents an evolutionary adaptation to extremely low Na^+ concentration of freshwater conditions.

Results

During a proteomic search for signaling components in zebrafish sperm (12), we identified peptides of a putative HCN channel, HCNL1 (*SI Appendix*, Fig. S1, National Center for Biotechnology Information [NCBI] accession number XP_002662296). A database search revealed 49 ortholog genes (*SI Appendix*, Table S1), all from fish, that form a subfamily of HCN channels (see Fig. 2*A*). The subfamily falls into two groups, HCNL1 and HCNL2. Heterologous expression of the cloned zebrafish HCNL1 gene in CHO cells gave rise to hyperpolarization-activated currents (Fig. 1*A*) that were similar to currents carried by classic HCN channels in the heart and brain (3, 13). The voltage dependence of HCNL1 activation was determined from tail currents recorded

Significance

We discovered a subfamily of voltage-gated ion channels, called HCN-like channels, consisting of two members, HCNL1 and HCNL2. In contrast to classic pacemaker HCN channels in the heart and brain, HCNL1 conducts protons rather than potassium or sodium ions. The pore domain, which exists in most voltage-gated channels, is nonconducting. Instead, protons permeate the channel via the voltage-sensing domain involving the S4 motif. Key to proton conduction is a methionine residue that interrupts the regularly spaced series of arginine residues in S4. We show that fish sperm use this unusual ion pathway to create a hyperpolarization-gated proton influx that counterbalances an alkaline-activated K^+ channel.

Author contributions: S.F., U.B.K., R.S., and T.K.B. designed research; L.W., T.W., S.F., W.B., H.G.K., J.F.J., C.T., R.S., and T.K.B. performed research; R.F. contributed new reagents/analytic tools; L.W., T.W., S.F., R.S., and T.K.B. analyzed data; and L.W., T.W., U.B.K., R.S., and T.K.B. wrote the paper.

The authors declare no competing interest.

This article is a PNAS Direct Submission.

This open access article is distributed under Creative Commons Attribution-NonCommercial-NoDerivatives License 4.0 (CC BY-NC-ND).

[1]Present address: Department of Molecular and Cellular Physiology, Stanford University, Stanford, CA 94305.

[2]U.B.K., R.S., and T.K.B. contributed equally to this work.

[3]To whom correspondence may be addressed. Email: u.b.kaupp@caesar.de, reinhard.seifert@caesar.de, or thomas.berger@uni-marburg.de.

This article contains supporting information online at https://www.pnas.org/lookup/suppl/doi:10.1073/pnas.2001214117/-/DCSupplemental.

First published May 28, 2020.

Downloaded at DKFZ-HGF on November 13, 2020

at −65 mV (Fig. 1*B*). Currents were half maximal at $V_{1/2} = -98.8 \pm 6.8$ mV with a slope $s = 5.8 \pm 1.5$ mV (mean ± SD, $n = 6$ experiments). However, although it carries a CNBD, HCNL1, unlike any other HCN channel, was insensitive to cyclic nucleotides (cAMP: $V_{1/2} = -96.6 \pm 3.6$ mV, $s = 6.6 \pm 1.3$ mV, $n = 5$; cGMP: $V_{1/2} = -100.1 \pm 3.0$ mV, $s = 5.8 \pm 1.2$ mV, $n = 6$).

The HCNL1 Channel Is Selective for Protons. We determined the ion selectivity of HCNL1 from the reversal potential (V_{rev}) of tail currents, which is diagnostic of the permeant ions. Surprisingly, tail currents behaved anomalously: upon prolonged stimulation, tail currents changed from inward to outward (*SI Appendix*, Fig. S2), suggesting that either the ion selectivity of HCNL1 is changed or ions are redistributed at the membrane (accumulation or depletion). Because of their low concentration, protons are particularly prone to redistribution during proton channel activity (14). To test whether HCNL1 conducts protons, we recorded currents from HCNL1- and HCN2-expressing (control) CHO cells and simultaneously measured intracellular pH (pH_i) using the fluorescent pH dye BCECF (2',7'-bis-(2-carboxyethyl)-5-(and-6)-carboxyfluorescein). Activation of HCNL1, but not HCN2 (a classic HCN channel), acidified the cell cytoplasm (Fig. 1*C*), showing that, indeed, protons permeate HCNL1.

To rigorously establish the proton selectivity of HCNL1, we measured V_{rev} using solutions previously used for the study of proton-selective channels (15–17). The solutions contain high pH buffer concentrations, which minimize proton redistribution, and large organic cations instead of alkali metal ions (15–17). Even under these conditions, large HCNL1 currents were still observed. The V_{rev} at defined pH differences (ΔpH = extracellular pH [pH_o] − intracellular pH [pH_i]) behaved as predicted from the Nernst equation (Fig. 1 *D* and *E*), indicating that only protons pass HCNL1. We also tested the selectivity for protons over other ions by comparing V_{rev} in the presence of the large, impermeant organic cation $NMDG^+$ versus various alkali ions. Exchanging $NMDG^+$ with alkali ions (at $pH_o = 6.5$, $pH_i = 5.5$) did not change V_{rev} significantly (Fig. 1*F*), demonstrating that the HCNL1 channel is exquisitely selective for protons. Cl^- also did not change V_{rev} (Fig. 1*F*). To determine the relative permeability of H^+ vs. Na^+ quantitatively, we reduced the H^+ concentration ($pH_i = pH_o = 7$) and recorded reversal potentials in HCNL1-expressing CHO cells. Here, a shift in V_{rev} could be observed: Replacing $NMDG^+$ with Na^+ resulted in a ΔV_{rev} of 7.2 ± 2.6 mV. According to the Goldman–Hodgkin–Katz (GHK) equation (18), the relative permeability of protons to sodium is $\frac{P_{H+}}{P_{Na+}} = 3 \times 10^6$.

HCNL1 from the common carp *Cyprinus carpio* and the goldfish *Carassius auratus* also mediated proton currents (*SI Appendix*, Fig. S3), suggesting that HCNL1 channels represent a family of hyperpolarization-activated proton channels.

HCNL1 Conducts Protons via the VSD. We set out to identify the proton permeation pathway in HCNL1. In voltage-gated ion channels, except the depolarization-activated proton channel H_v1, a stretch of conserved residues in the PD comprises the selectivity filter of the pore (19, 20). In classic HCN channels, a short conserved CIGYG sequence motif in the pore loop determines the ion selectivity (Fig. 2 *B*, yellow). Mutations in this motif abolish ion conduction in HCN channels (21). This canonical CIGYG motif is absent in HCNL1 channels, and the corresponding string of amino acid residues is not conserved among HCNL1 channels from different species (WPFLE in drHCNL1, WISTK in caHCNL1 and ccHCNL1) (Fig. 2*B* and *SI Appendix*, Table S1). This comparison suggests that the PD in HCNL1 channels is nonconducting, and protons might permeate via another pathway.

In Na^+ and K^+ channels, mutations that introduce gaps in the regular spacing of the S4 Arg residues in the VSD can induce pores (22–25). The resulting currents through the VSD have been termed "gating pore currents" or "omega currents." A

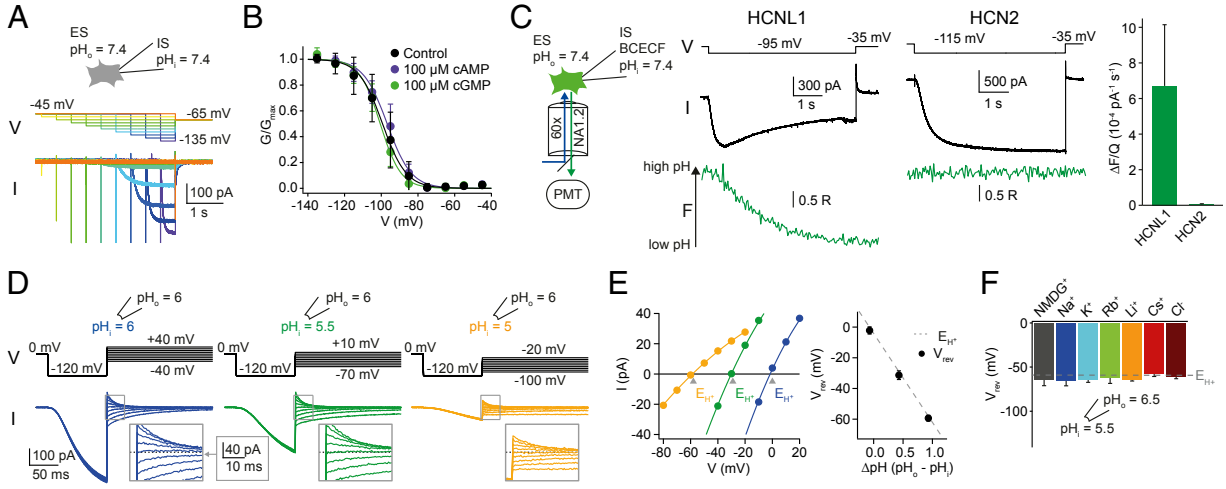

Fig. 1. Zebrafish HCNL1 is a proton-selective channel. (*A*) Whole-cell patch clamp recording of zebrafish HCNL1-expressing CHO cells. Voltage steps of increasing length and decreasing amplitude (color-coded, −135 to −45 mV in 10 mV increments) elicited voltage-dependent inward currents. (*B*) Conductance–voltage relationships (GVs) derived from tail currents of HCNL1-expressing CHO cells without (black) or with 100 µM intracellular cAMP (purple) or cGMP (green). (*C*) Whole-cell patch clamp fluorometry recording of zebrafish HCNL1- or mouse HCN2-expressing CHO cells, filled with the pH indicator BCECF. The bar graph shows the mean ratio of the fluorescence amplitude over the transported charge of zebrafish HCNL1- or mouse HCN2-expressing cells (HCNL1, $6.7 \times 10^{-4} \pm 3.4 \times 10^{-4}$ pA^{-1} s^{-1}, $n = 9$; HCN2, $5.1 \times 10^{-6} \pm 3.2 \times 10^{-6}$ pA^{-1} s^{-1}, $n = 5$). (*D*) Excised inside-out patch clamp recording from *X. laevis* oocytes expressing HCNL1 measured at three different pH_i. (*E*, *Left*) Current–voltage relationships of the tail currents in *D*. E_{H+} is the Nernst potential for protons at different ΔpH. (*E*, *Right*) Reversal potential as a function of ΔpH (ΔpH = 1: $V_{rev} = -59.4 \pm 1.9$ mV, $n = 6$; ΔpH = 0.5: $V_{rev} = -31.3 \pm 2.9$ mV, $n = 12$; ΔpH = 0: $V_{rev} = -2.2 \pm 2.4$ mV, $n = 15$). The dashed line represents E_{H+}. (*F*) Reversal potential in response to bath application of various cations (90 mM) or chloride (40 mM) with $pH_i = 5.5$ and $pH_o = 6.5$ ($E_{H+} = -58.6$ mV), measured in excised inside-out patches from *X. laevis* oocytes expressing HCNL1 ($NMDG^+$: −64.3 ± 6.7 mV, $n = 9$; Na^+: −65.7 ± 5.6 mV, $n = 5$; K^+: −64.4 ± 2.8 mV, $n = 5$; Rb^+: −62.1 ± 6.5 mV, $n = 6$; Li^+: −63.6 ± 2.0 mV, $n = 4$; Cs^+: −57.1 ± 3.6 mV, $n = 5$; Cl^-: −61.9 ± 1.5 mV, $n = 3$). ES, extracellular solution; IS, intracellular solution; PMT, photomultiplier tube. Error bars denote SD.

Downloaded at DKFZ-HGF on November 13, 2020

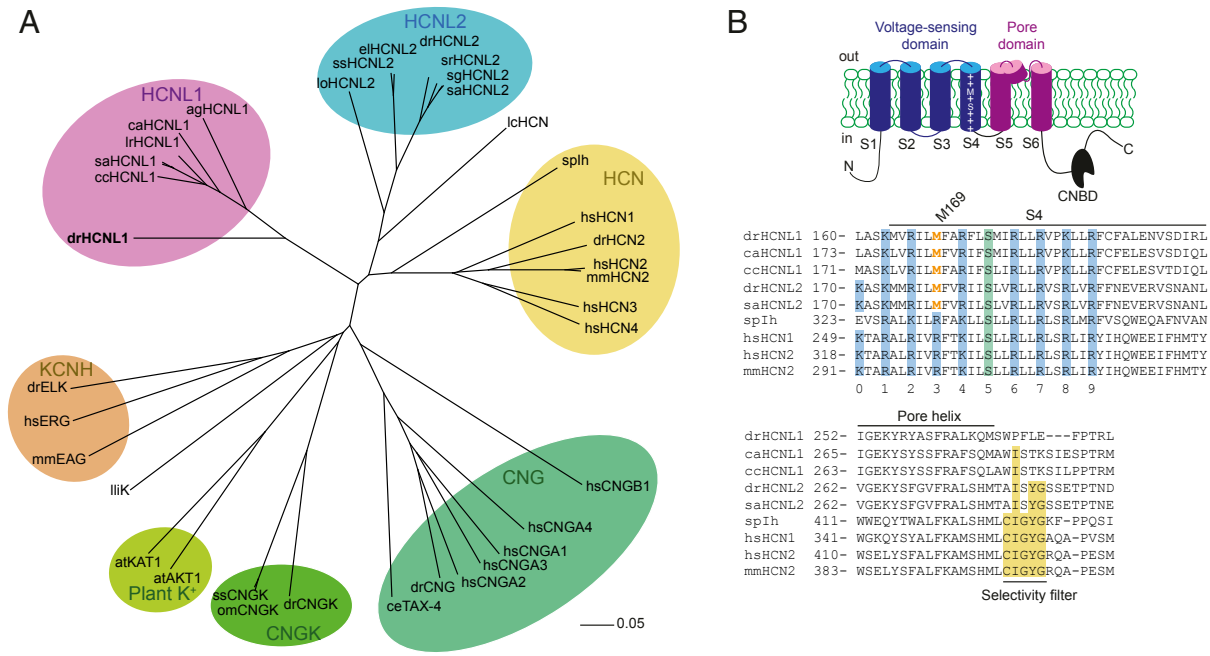

Fig. 2. Structural features of the zebrafish HCNL1 channel. (*A*) Phylogenetic tree of ion channels containing a CNBD (accession numbers of HCNL1/2 channels are listed in *SI Appendix*, Table S1). The scale bar represents 0.05 substitutions per site. (*B*, *Top*) Cartoon of HCNL1. (*B*, *Bottom*) Alignment of S4 transmembrane helices and pore domains of the HCNL1/2 and HCN channels.

number of pathologic conditions, termed "channelopathies," are caused by channels with these gating pore currents (25). Probably by a related mechanism, H_v1 conducts protons through its VSD because it lacks a central PD (15, 16). Mutations of the S4 segment of H_v1 abolish proton permeation (17, 26, 27) or alter ion selectivity (28). Therefore, we compared the S4 sequences of HCN, HCNL1/2, and H_v1 channels with emphasis on interruptions of the Arg residue pattern. The S4 segment of classic HCN and HCNL1/2 channels is highly conserved: It carries a string of up to eight regularly spaced Arg residues that is interrupted in both channel types at the fifth position by a serine residue (Fig. 2*B*). Strikingly, in HCNL1/2 but not classic HCN channels, the string of Arg residues is additionally interrupted at the third position by a methionine residue (M169 in zebrafish HCNL1) (Fig. 2*B*). The S4 segment of H_v1, compared to that of the HCN and HCNL1/2 channels, contains a shorter string of positively charged residues, consisting of only three Arg residues.

Four experimental observations argue that the VSD represents the proton permeation pathway in HCNL1. First, pharmacological experiments support the notion that protons permeate through the VSD rather than the PD (Fig. 3*A*). The open-channel blocker ZD7288 of classic HCN channels did not block HCNL1 currents (Fig. 3*B*), although hydrophobic amino acid residues important for drug binding (29) are conserved in HCNL1 (Fig. 3*A*). By contrast, an open-channel blocker of H_v1 channels, 2-guanidinobenzimidazole (2GBI) (30, 31), and its membrane-permeable congener 5-chloro-2-guanidinobenzimidazole (ClGBI), both blocked HCNL1 (but not classic HCN2) currents in a dose-dependent fashion (Fig. 3 *B* and *C*). A key feature of VSDs is a conserved phenylalanine in the transmembrane segment S2 referred to as a gating charge transfer center (32). Mutation of the respective Phe to Ala in H_v1 leads to an increase of the efficacy of 2GBI (30). Mutating the homologous Phe in HCNL1 to Ala (F96A) also changes the efficacy of 2GBI; however, in the HCNL1 context, the affinity of the mutant was lower (Fig. 3*C*). In both channel types, the conserved Phe residue of the gating charge transfer center participates in the binding of GBI compounds. In summary, these results suggest that GBI compounds block HCNL1 currents by occluding a proton permeation pathway in the VSD.

Second, we examined whether the PD of HCNL1 channels contributes to ionic currents. Various constructs lacking the PD were nonfunctional (*SI Appendix*, Fig. S4). Therefore, we took a less invasive strategy: in HCN channels, replacing the canonical selectivity filter GYG by AAA produces nonconducting, dominant-negative channels (21). We constructed a congruous HCNL1 mutant in which the respective amino acids (FLE; positions 271 to 273) (Fig. 2*B*) were replaced by AAA (HCNL1-AAA). In this functional mutant, proton permeation and selectivity were not altered (Fig. 3 *D*–*F*), suggesting that the proton permeation pathway of HCNL1 does not involve the central PD.

Third, we investigated a channel mutant where M169 in the S4 segment was replaced by an Arg residue (M169R). Thereby, we generated a sequence of charges in S4 that is similar to that of classic HCN channels that do not transport ions via S4 (Fig. 2*B*). This mutant, in inside-out patches from *Xenopus* oocytes, carried only small transient currents, much smaller than the currents that we robustly obtained for wild-type channels (Fig. 4*A*). Low expression of the mutant was not responsible for the small current because patch clamp fluorometry of GFP-tagged variants of wild-type and M169R channels demonstrated similar expression levels, despite large differences in patch current (Fig. 4 *B* and *C*). We studied the M169R mutant in more detail in CHO cells. Here, in whole-cell recordings, the transient currents were larger and robust (Fig. 4*D*). We reasoned that the transient currents could either originate from fast channel inactivation or might represent gating currents due to S4 movement across the electric field of the membrane. To discriminate between the two possibilities, we activated M169R channels and, when the peak current was reached, stepped to various voltages from −80 to +80 mV under symmetric ion concentrations (Fig. 4 *E*, *Left*). Under these conditions, ionic currents, but not gating currents, are expected to reverse direction at V_{rev} = 0 mV. However, currents did not reverse (Fig. 4 *E*, *Right*), a behavior incompatible with ionic currents. Currents also did not reverse under Na^+- and K^+-based solutions (Fig. 4 *E*, *Right*). We conclude that the residual currents produced by the

Downloaded at DKFZ-HGF on November 13, 2020

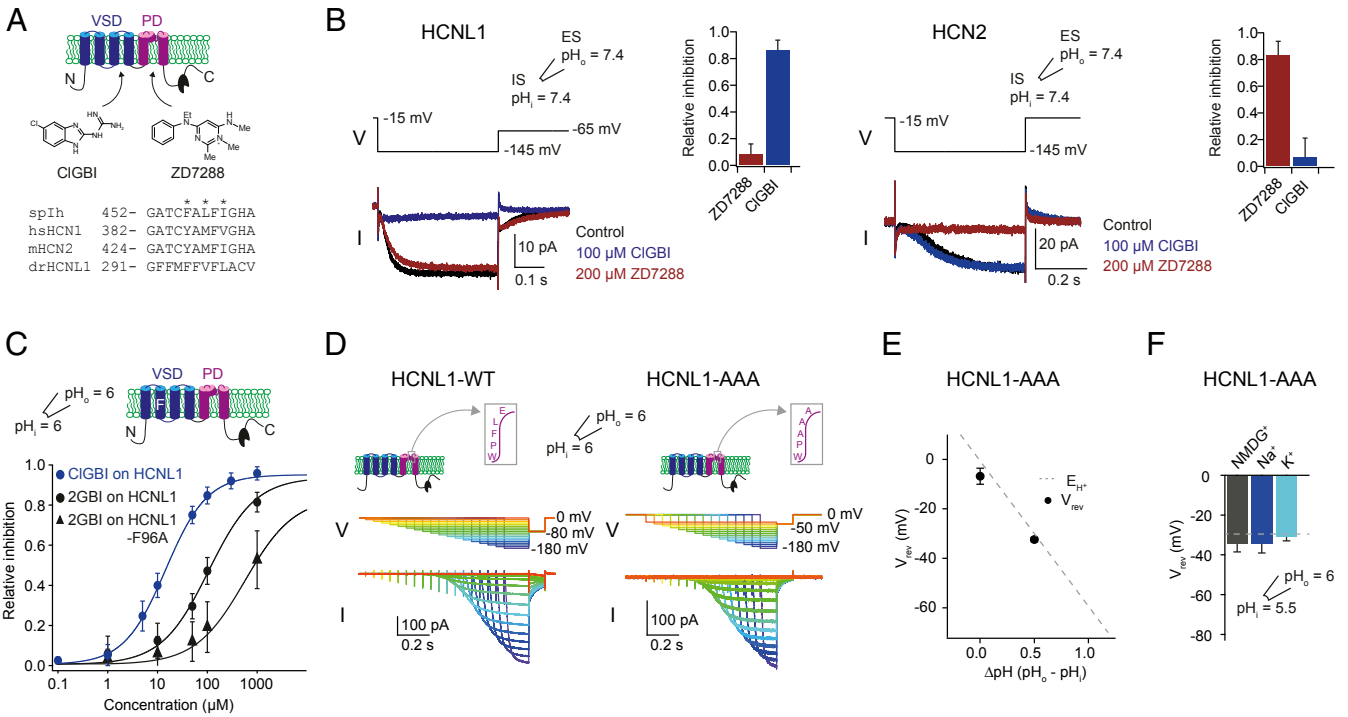

Fig. 3. Blockers of the VSD, but not of the PD, inhibit HCNL1. (*A*, *Top*) Cartoon of HCNL1 as a potential target of H_v1 blocker ClGBI and HCN blocker ZD7288. (*A*, *Bottom*) Alignment of part of transmembrane segment S6 that contains amino acid residues crucial for binding of ZD7288 in spIh. (*B*) Excised inside-out patch clamp recording from a zebrafish HCNL1-expressing CHO cell (*Left*) and a mouse HCN2-expressing HEK cell (*Right*) in the presence or absence of 100 µM ClGBI (blue) or 200 µM ZD7288 (dark red). Bar graphs show the mean relative inhibition of zebrafish HCNL1 and mouse HCN2 in response to ZD7288 and ClGBI. (*C*) Dose–response curve and Hill fit of 2GBI and ClGBI on wild-type HCNL1 (2GBI: half maximal inhibitory concentration [IC_{50}] = 106 ± 22 µM, Hill coefficient [h] = 0.9 ± 0.4, n = 4; ClGBI: IC_{50} = 14 ± 3 µM, h = 1.1 ± 0.1, $n \geq 5$ for each data point) and 2GBI on HCNL1-F96A (IC_{50} = 568 ± 413 µM, h = 0.9 ± 0.3, $n \geq 4$ for each data point), recorded in excised inside-out patches from *X. laevis* oocytes. (*D*) Excised inside-out patch clamp recording from *X. laevis* oocytes expressing HCNL1 (*Left*) or HCNL1-AAA (*Right*). (*E*) Reversal potential of currents from HCNL1-AAA as a function of ΔpH (ΔpH = 0: V_{rev} = −6.8 ± 3.3 mV, n = 5; ΔpH = 0.5: V_{rev} = −32.4 ± 0.9 mV, n = 5). The dashed line represents E_{H+}. (*F*) Effect of bath application of various cations (90 mM) on the reversal potential with pH$_i$ = 5.5 and pH$_o$ = 6 (E_{H+} = −29.3 mV), measured in excised inside-out patches from *X. laevis* oocytes expressing HCNL1-AAA ($NMDG^+$: −34.6 ± 3.9 mV, n = 5; Na^+: −34.6 ± 4.4 mV, n = 5; K^+: −30.8 ± 2.2 mV, n = 5). Error bars denote SD.

M169R mutant predominantly represent gating currents. The charge–voltage relationships, obtained by integrating on- and off-gating currents, saturated, and their voltage dependence was similar (Fig. 4*F*). On-gating charges of HCNL1 were much larger than off-gating charges (Fig. 4*F*). A similar behavior of H_v1 and Shaker K^+ channels has been attributed to a phenomenon called "voltage sensor immobilization" (27, 33). During prolonged activation, the voltage sensor enters a more stable conformation from which it recovers only slowly. This immobilization results in an apparent loss of off- compared to on-gating charges. Voltage sensor immobilization is initially small and increases during long stimulation times. Therefore, we recorded on- and off-gating currents of HCNL1 for different pulse lengths. For short stimulation times, on- and off-gating charges were similar (Fig. 4*G*). With longer stimulation times, the ratio of off- to on-gating charges decayed exponentially (τ_{decay} = 50.6 ± 8.3 ms, n = 5, Fig. 4*G*), which is diagnostic for voltage sensor immobilization. In summary, in the M169R mutant, proton currents are suppressed, and gating currents become apparent, suggesting that M169 lines the pore.

Fourth, we mutated M169 to cysteine, which can be chemically modified with 2-(trimethylammonium)ethyl methanethiosulfonate (MTSET). Activation of the M169C mutant produced proton currents that were blocked by MTSET modification; the wild-type HCNL1 control was not affected by MTSET (Fig. 4*H*). Collectively, these results show that protons pass HCNL1 via the VSD and M169 lines the proton permeation pathway; furthermore, the "classic" central pore region of HCNL1 does not pass protons or alkali metal ions.

HCNL1 Mediates Hyperpolarization-Activated Currents in Zebrafish Sperm. Next, we studied the native HCNL1 channel in zebrafish sperm by whole-cell patch clamping. In a Cs^+-based solution, which eliminates K^+ currents carried by the K^+-selective cyclic-nucleotide-gated channel (CNGK) (12), we recorded hyperpolarization-activated currents that were similar to currents of heterologously expressed HCNL1 ($V_{1/2}$ = −105.3 ± 11.4 mV, s = 13.0 ± 2.1, n = 5) (Fig. 5*A*). These currents were also not cyclic nucleotide sensitive (cAMP: $V_{1/2}$ = −100.6 ± 17.2 mV, s = 11.0 ± 2.6 mV, n = 4; cGMP: $V_{1/2}$ = −110.0 ± 6.6 mV, s = 10.0 ± 2.6 mV, n = 3). Furthermore, during current activation, the fluorescence of the pH dye pHrodo Red increased (Fig. 5*B*, 5.3 × 10^{-3} ± 1.9 × 10^{-3} pA^{-1} s^{-1}, n = 8), indicating acidification by proton flux into sperm. Finally, ClGBI (100 µM) blocked the inward current in sperm (Fig. 5*C*, 73 ± 9%, n = 4). These results show that HCNL1 mediates hyperpolarization-activated currents in zebrafish sperm.

HCNL1 Forms Tetramers and Is Expressed in the Head of Zebrafish Sperm. We examined the presence of HCNL1 protein in zebrafish sperm by two independent monoclonal antibodies directed against N- (anti-N_{term}) and C-terminal (anti-C_{term}) epitopes of HCNL1. In Western blots of HCNL1-HA-injected oocytes, anti-HCNL1 and anti-HA antibodies labeled a polypeptide with an apparent molecular weight (M_w) of about 62 kDa, similar to the

Downloaded at DKFZ-HGF on November 13, 2020

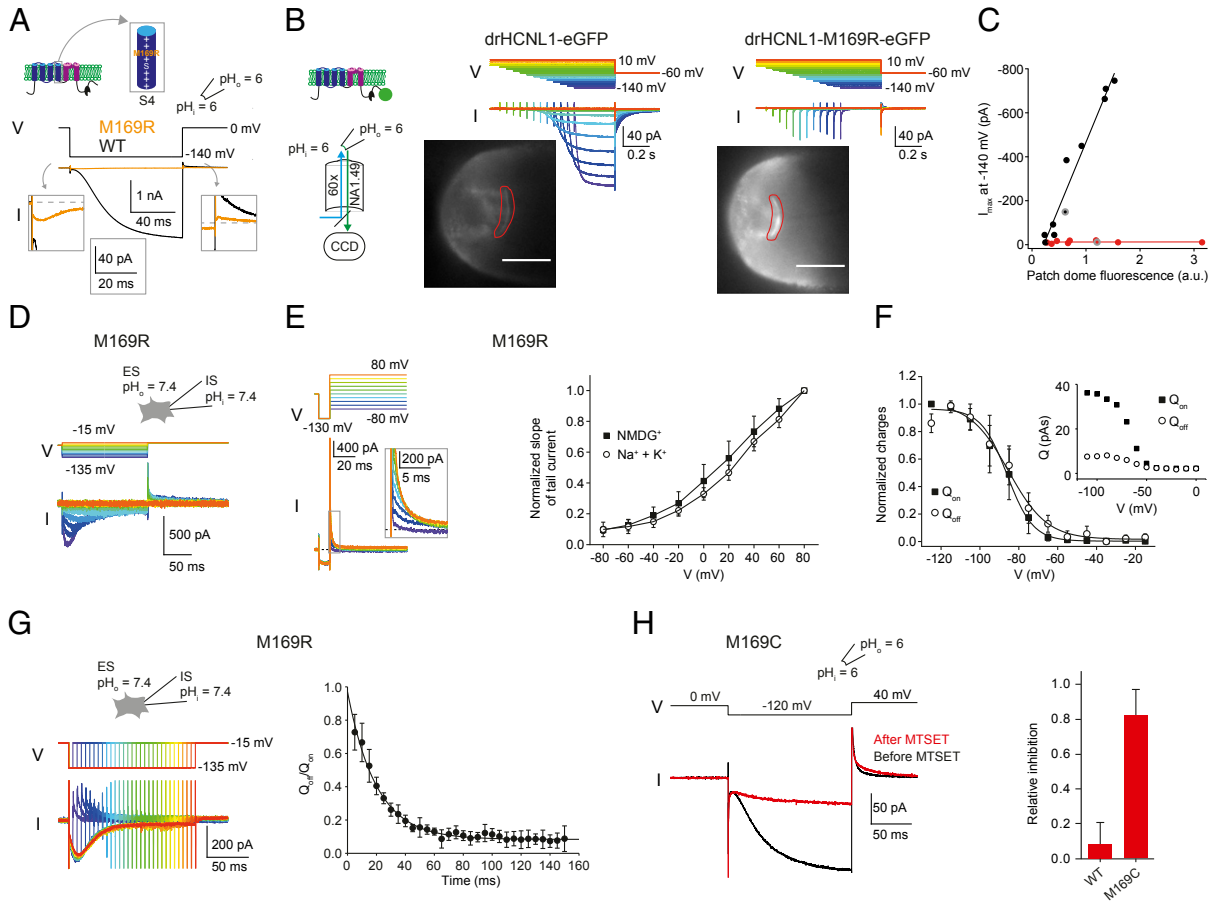

Fig. 4. Position M169 in the S4 segment is key for proton permeation in HCNL1. (*A*) Excised inside-out patch clamp recordings from *X. laevis* oocytes expressing wild-type HCNL1 (black) or mutant HCNL1-M169R (orange). (*B*) Excised inside-out patch clamp recording from a *X. laevis* oocyte expressing HCNL1-eGFP (*Left*) or HCNL1-M169R-eGFP (*Right*). eGFP was excited by cyan light; the images of the patch pipettes were recorded under identical illumination and exposure time. The patch domes are encircled by a red trace. (Scale bars, 20 μm.) (*C*) Maximal (negative) current (I_{max}) recorded at −140 mV as a function of the patch dome fluorescence (black, HCNL1-eGFP; red, HCNL1-M169R-eGFP). Lines are linear fits (black, slope $s = 5.9 \times 10^{-4}$ pA/F; red, $s = 5.6 \times 10^{-7}$ pA/F). Data from patches shown in *B* are encircled in gray. (*D*) Whole-cell patch clamp recording of a CHO cell expressing HCNL1-M169R. (*E*, *Left*) Whole-cell patch clamp recording of CHO cells expressing HCNL1-M169R. (*E*, *Right*) Normalized slopes of the tail current as a function of the voltage for HCNL1-M169R, measured in symmetric $NMDG^+$- or Na^+/K^+-based solutions. (*F*) Normalized charge–voltage relationship (QV) of HCNL1-M169R derived from *D* ("on," $V_{1/2} = -86.4 \pm 5.0$ mV, $s = 6.7 \pm 0.5$ mV; "off," $V_{1/2} = -84.9 \pm 5.6$ mV, $s = 10.0 \pm 1.6$ mV, $n = 6$). (*Inset*) QV of HCNL1-M169R showing fourfold larger on than off currents. (*G*, *Left*) Whole-cell patch clamp recording of a CHO cell expressing HCNL1-M169R. (*G*, *Right*) Ratio Q_{off}/Q_{on} as a function of stimulus duration. (*H*, *Left*) Excised outside-out patch clamp recording from *X. laevis* oocytes expressing HCNL1-M169C before (black) and after application of 1 mM MTSET (red). (*H*, *Right*) Relative inhibition of HCNL1-M169C (79.2 ± 15.2%, $n = 12$) and wild-type HCNL1 (8.1 ± 13.4%, $n = 5$) by MTSET. Error bars denote SD.

calculated M_w of 60.4 kDa (Fig. 6*A*). In Western blots of control oocytes, no band was detected, demonstrating the specificity of these antibodies. The antibodies also detected a smear between 65 and 75 kDa. Upon treatment with PNGase, the smear collapsed into a single 62-kDa band, suggesting that HCNL1 proteins are glycosylated (Fig. 6*B*). The anti-C_{term} antibody detected

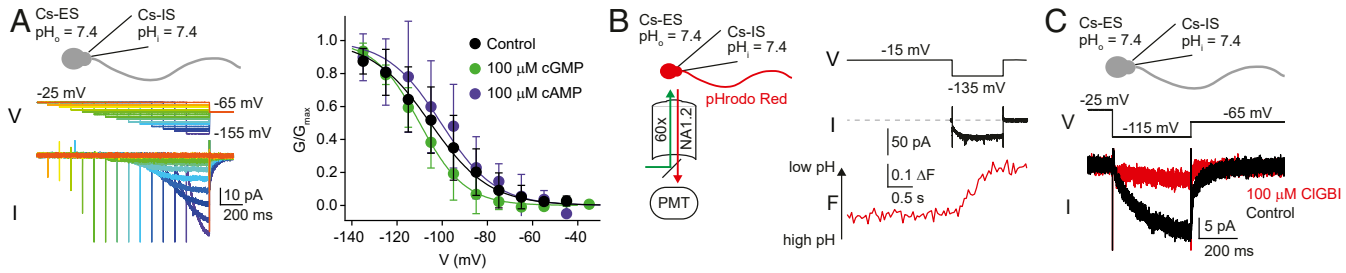

Fig. 5. HCNL1 acidifies zebrafish sperm upon hyperpolarization. (*A*, *Left*) Whole-cell patch clamp recording of hyperpolarization-activated currents in zebrafish sperm in the presence of Cs^+ to block CNGK. (*A*, *Right*) GVs derived from tail currents with or without 100 μM cAMP or cGMP in the intracellular solution. Error bars denote SD. (*B*) Whole-sperm patch clamp fluorometry recording with the fluorescent pH indicator pHrodo Red. (*C*) Block of hyperpolarization-activated current in zebrafish sperm by 100 μM ClGBI (73 ± 9%, $n = 4$). Error bars denote SD.

Downloaded at DKFZ-HGF on November 13, 2020

HCNL1 protein in tissue of zebrafish testis and in zebrafish sperm (Fig. 6*B*) but not in the ovary, eyes, and brain (*SI Appendix*, Fig. S5*A*); PNGase treatment also lowered the M_w of HCNL1 in testis and sperm (Fig. 6*B*).

Classic HCN channels are composed of four subunits that form a single pore (34), whereas H_v1 forms a dimer (35, 36) with two proton pores (17). In Western blots of chemically cross-linked HCNL1 protein, bands at 59.3, ~120, ~180, and ~240 kDa were detected. The higher molecular species are multiples of the monomer (*SI Appendix*, Fig. S5*B*), suggesting a tetrameric organization. Thus, each HCNL1 channel probably carries four proton pores (*SI Appendix*, Fig. S5*C*).

We studied the cellular distribution of HCNL1 in sperm by immunocytochemistry. The anti-N_{term}, anti-C_{term}, and anti-HA antibodies stained HCNL1-HA-transfected but not control CHO cells, demonstrating that these antibodies are suitable for immunocytochemistry (Fig. 6 *C* and *D*). Both anti-HCNL1 antibodies stained heads from zebrafish sperm, whereas the flagellum was only weakly recognized (Fig. 6 *E* and *F*). Moreover, currents recorded from isolated sperm heads and from

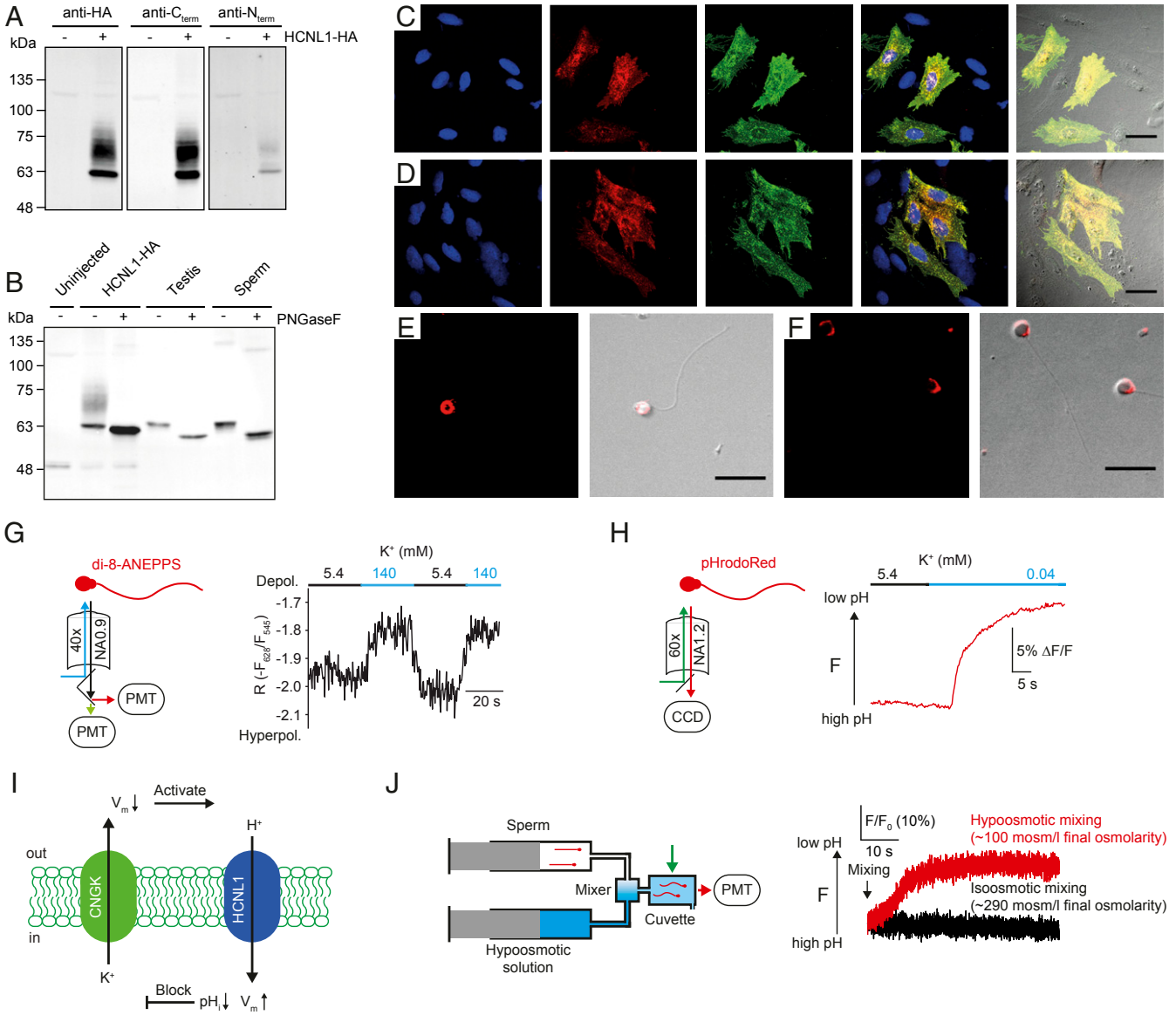

Fig. 6. HCNL1 is located in the sperm head and is functionally connected to the CNGK channel. (*A*) Western blot of *X. laevis* oocytes expressing HCNL1-HA using an HA antibody or an anti-C_{term} or anti-N_{term} antibody against HCNL1. Molecular weight standards are indicated on the left. (*B*) Western blot of uninjected *X. laevis* oocytes, oocytes expressing HCNL1-HA, testis tissue, and sperm using the anti-C_{term} antibody and in the presence or absence of PNGaseF. (*C* and *D*) Immunocytochemical staining of a mixture of control and zebrafish HCNL1-HA-expressing CHO cells (blue, DAPI; red in *C*, anti-C_{term} antibody with Cy3; red in *D*, anti-N_{term} antibody with Cy3; green, mouse anti-HA antibody with Alexa488; merged fluorescence channels; Cy3 and Alexa488 merged with bright-field illumination). (Scale bars, 25 μm.) (*E* and *F*, *Left*) Immunocytochemical staining of zebrafish sperm using the anti-C_{term} (*E*) or anti-N_{term} (*F*) antibody. (*E* and *F*, *Right*) Same staining as in the *Left*, overlaid with bright-field illumination. (Scale bars, 10 μm.) (*G*) Fluorescence recording of zebrafish sperm loaded with the fluorescent voltage-sensitive dye di-8-ANEPPS, superfused with regular ES (5.4 mM K^+), followed by wash in of an ES containing 140 mM K^+ (replacing Na^+). (*H*) Fluorescence recording of a single zebrafish sperm cell loaded with the fluorescent pH indicator pHrodo Red, superfused with regular ES (5.4 mM K^+), followed by wash in of an ES containing only 0.04 mM K^+. Fluorescence increases, indicating intracellular acidification. (*I*) Cartoon of the putative interplay between CNGK and HCNL1 channels. (*J*) Rapid mixing of pHrodo Red–loaded zebrafish sperm with standard ES (black trace) or a hypoosmotic solution (red trace) in a stopped-flow apparatus. Traces are the mean of three sweeps.

Downloaded at DKFZ-HGF on November 13, 2020

whole sperm were similar in amplitude (*SI Appendix*, Fig. S6). Thus, HCNL1 is predominantly localized to the sperm head. This finding is remarkable because CNGK, the only other ion channel identified in zebrafish sperm, is also localized to the head (12).

HCNL1 Is Functionally Linked to the K^+ Channel CNGK. Finally, we addressed the physiological role of HCNL1. We previously identified in zebrafish sperm the K^+-selective CNGK channel (12). CNGK is pH dependent: At alkaline pH, CNGK opens, and at acidic pH, CNGK closes. Current clamp recordings from zebrafish sperm show that intracellular alkalization hyperpolarizes the membrane potential, suggesting that CNGK is involved in setting the resting membrane potential (12). We confirm here the K^+ dependence of the resting membrane potential in single sperm cells loaded with the fluorescent voltage-sensitive dye di-8-ANEPPS (4-(2-[6-(dioctylamino)-2-naphthalenyl]ethenyl)-1-(3-sulfopropyl)pyridinium): When external K^+ was high, like in the seminal fluid of most freshwater fish species (37), the membrane potential was depolarized; when external K^+ was low, like in fresh water, the membrane potential was more hyperpolarized (Fig. 6*G*). Next, we tested whether hyperpolarization by low extracellular K^+ concentrations also activates HCNL1. Indeed, reducing the extracellular K^+ concentration from 5.4 mM to 40 μM leads to intracellular acidification (Fig. 6*H*, 8.8 ± 5.1% ΔF/F, see *SI Appendix*, *Materials and Methods* for details, $n = 22$), suggesting that hyperpolarization by CNGK activates HCNL1, which leads to subsequent proton influx. In turn, proton influx through HCNL1 decreases pH_i and thereby should lower the open probability of the pH-sensitive CNGK. The reciprocal interaction of the two channels creates an intricate negative feedback loop (Fig. 6*I*). In conclusion, the HCNL1 function in zebrafish sperm is similar to that of classic HCN channels: It limits hyperpolarization and initiates recovery from hyperpolarization.

Upon spawning into fresh water, sperm are exposed to a hypoosmotic shock, which eventually activates motility. We emulated a hypoosmotic shock during spawning by rapid mixing in a stopped-flow device pHrodo Red-loaded sperm in isoosmotic solution with a hypoosmotic solution. Changes in pH_i were detected by changes in fluorescence of the pH-sensitive dye. Challenging sperm with such a hypoosmotic shock triggered a decrease of pH_i (Fig. 6*J*, 12.1 ± 4.5% $\Delta F/F_0$, $n = 5$). These experiments suggest a role of HCNL1 during sperm activation.

Discussion

HCNL1 is the founding member of a family of hyperpolarization-activated channels that are highly selective for protons; only three other proton channels have been identified: H_v1 and Otopetrin in eukaryotes (15, 16, 38) and M2 in the influenza virus (39, 40).

Although HCNL1 channels and classical HCN channels are highly homologous, two specific modifications have completely changed their physiology. First, the PD of the channel carries mutations that "plug the pore." The central pore, key to ion permeation in all other members of voltage-gated ion channels, is nonfunctional in HCNL1. Second, replacing a single arginine, present in the S4 segment of all classic HCN channels, by methionine (M169 in drHCNL1) endows HCNL1 with proton permeability. How do protons pass the VSD in HCNL1? The VSD of classic voltage-gated channels adopts an hourglass shape with a central hydrophobic constriction site (HCS) that is formed by hydrophobic residues in segments S1 to S3 and that separates the extra- from the intracellular side (32, 41–43). During activation, the voltage-sensing S4 segment travels through the HCS. While S4 moves, the constriction is always occupied by one of the positively charged residues of S4, and no ions can pass the HCS. However, mutations of Arg residues in S4 of K_v, Na_v, and Ca_v channels can cause voltage-dependent currents flowing through the VSD, so-called gating pore currents (22–25). Some of these mutants have been identified in human voltage-gated channels that give rise to nonselective currents through the VSD and cause channelopathies (25). A similar mechanism may give rise to proton currents in HCNL1, with the major difference that the currents through HCNL1 are exquisitely proton selective. We envision that hyperpolarization might relocate M169 to the VSD constriction site and thereby generate a proton-selective pore. Remarkably, introducing at position M169 an Arg residue that "fills the gap" in the string of regularly spaced Arg residues abolishes proton permeation, and gating currents become apparent. Similarly, in H_v1, an Arg residue introduced at the fourth S4 position in register with the three other Arg residues blocks proton permeation (17) and reveals gating currents (26, 27). In this respect, HCNL1 and H_v1 seem to share a common mechanism of proton permeation. For H_v1, the mechanism of proton permeation is not completely understood and is debated in the community (44, 45). The discovery of a second channel possessing an analogous, yet hyperpolarization-activated, proton permeation pathway will give ample opportunities to gain insight into the requirements for proton pores in VSDs.

V_{rev} for proton currents is not affected by orders-of-magnitude higher concentrations of monovalent cations, suggesting a more than a millionfold higher permeability for protons than for other ions. In fact, the relative permeability of H^+ vs. Na^+ is 3×10^6. Proton selectivity of HCNL1 is therefore within the same order of magnitude as that of the H_v1 proton channel (46). Channels that conduct ions through a classic PD typically feature a much lower selectivity (P_{K+}:P_{Na+} = 1,000 to 10,000 for K^+ channels and P_{Na+}:P_{K+} = 100 to 500 for Na^+ channels) (18). Given the extremely low concentration of protons in most physiological environments (10^{-7} to 10^{-8} M), this exquisite proton selectivity is essential for HCNL1 to actually function as a proton-conducting channel (21).

The pore sequence of HCNL2 is more conserved than that of HCNL1: HCNL2 channels carry AISYG, QISYG, or ALSYG sequence motifs (*SI Appendix*, Table S1), which is similar to the canonical CIGYG motif of classic HCN channels. In K_v channels, however, the analogous Gly to Ser exchange at the first position of the GYG motif renders the K_v pore nonconducting (47), and a CISYG sequence in human HCN4 results in nonconducting, dominant negative subunits (48), suggesting that the pore of HCNL2 might be nonfunctional as well. All HCNL2 channels carry the characteristic Met in S4 that is crucial for proton conduction in HCNL1. Therefore, we speculate that HCNL2 also conducts protons via the same VSD pathway. Functional expression of HCNL2 in heterologous systems was unsuccessful. HCNL2 transcripts are enriched in zebrafish hair cells (49).

Zebrafish sperm become activated by hypoosmotic shock during the release into fresh water. After activation, sperm have about 1 min to find the egg and the micropyle, a tiny hole in the chorion of the egg through which the sperm can reach the plasma membrane for fertilization. The molecular signaling pathways that control the sperm's journey to the egg are not known.

Fresh water is extremely low in Na^+ and K^+ (0.1 to 0.7 mM). Not much is known about the ion channel inventory of zebrafish sperm, except for the alkaline-activated, K^+-selective CNGK channel (12). CNGK is active under resting conditions and closes upon intracellular acidification (12). HCNL1 is the second channel type identified in zebrafish sperm. CNGK and HCNL1 are both present in the sperm head. Classic HCN channels in the heart and brain carry a Na^+ inward current that depolarizes the cell. However, because of the low Na^+ and K^+ concentrations of fresh water, HCN channels instead would strongly hyperpolarize zebrafish sperm. The proton selectivity enables HCNL1 to depolarize cells in a freshwater environment. Thus, the hyperpolarization produced by the K^+-selective CNGK channel upon release into fresh water activates HCNL1; the ensuing proton

Downloaded at DKFZ-HGF on November 13, 2020

influx limits the hyperpolarization in two ways: 1) Proton influx directly depolarizes the membrane potential, and 2) the intracellular acidification will close CNGK channels. Although CNGK and HCNL1 carry a CNBD, both channels are insensitive to cyclic nucleotides, suggesting that protons instead of cyclic nucleotides serve as cellular messengers in zebrafish sperm.

Across phyla, Ca^{2+} ions control sperm motility and navigation (50). The sperm-specific Ca^{2+} channel CatSper mediates Ca^{2+} influx in many but not all species from marine invertebrates to humans. Some teleost fish, including zebrafish, and birds and amphibians lack CatSper channels (51). The channel(s) and mechanisms that promote voltage-activated Ca^{2+} influx in CatSper-deficient sperm are not known. In marine invertebrates, the interplay between hyperpolarization, alkalization, and, ultimately, depolarization activates CatSper channels (52, 53). The opening of K^+-selective, cyclic nucleotide-gated CNGK channels hyperpolarizes sperm; HCN channels counteract hyperpolarization. During recovery from hyperpolarization, CatSper channels open. We hypothesize that, in zebrafish sperm, a similar interplay between the pH-sensitive CNGK and the proton-selective HCNL1 may control a voltage- and/or pH_i-gated Ca^{2+} conductance. The swimming pattern of zebrafish sperm depends on the intracellular Ca^{2+} concentration (12), and Ca^{2+} signaling might be crucial for successful navigation to the micropyle. We speculate that activation of CNGK and HCNL1 during spawning changes the intracellular Ca^{2+} concentration and thereby activates and modulates sperm swimming. To further delineate the signaling pathway that controls zebrafish sperm motility and navigation, it will be necessary to identify additional molecular components that control the intracellular Ca^{2+} concentration.

Materials and Methods

Expression in CHO Cells and *X. laevis* Oocytes. For channel expression in *X. laevis* oocytes, oocytes were injected with mRNA obtained from in vitro transcription and incubated at 14 to 16 °C for 1 to 5 d. For channel expression in CHO cells, either a stable cell line was generated, or for transient expression, cells were transfected at least 24 h before use. Additional information on channel expression is provided in *SI Appendix, Materials and Methods*.

Biochemistry. Zebrafish sperm were solubilized using a hypotonic solubilization buffer and sonification. *X. laevis* oocytes were mechanically devitellinated and homogenized by trituration. Standard procedures were used for sodium dodecyl sulfate polyacrylamide gel electrophoresis (SDS/PAGE) and Western blot. Anti-HCNL1 antibodies were generated from stable rat hybridoma clones. Cross-linking was performed with the amino-specific cross-linker disuccinimidyl suberate. Additional information on biochemical protocols is provided in *SI Appendix, Materials and Methods*.

Electrophysiology and Fluorometry. Electrophysiological recording of CHO cells and *X. laevis* oocytes was performed using standard experimental procedures. For pH fluorometry, cells were loaded with the pH indicator BCECF. To record gating currents, online leak subtraction was applied using the p/4 protocol. In some cases, leak currents were subtracted off-line. Junction potentials were calculated with pClamp 10 and subtracted off-line. For whole-cell recordings of intact zebrafish sperm and isolated sperm heads, gigaseals were formed at the neck region of the sperm cell. For patch clamp fluorometry measurements of zebrafish sperm, sperm cells were loaded with the pH indicator pHrodo Red AM prior to recording. All electrophysiological measurements were performed at room temperature. Changes in pH_i of single zebrafish sperm in response to changes in the extracellular K^+ concentration (Fig. 5*B*) were measured by superfusing sperm loaded with pHrodo Red AM with solution containing different concentrations of K^+. The fluorescence signal was determined from the spatial average of a region of interest covering the sperm head. Additional information on electrophysiological and fluorometric recording procedures is provided in *SI Appendix, Materials and Methods*.

Immunocytochemistry. A stable CHO cell line expressing HCNL1-HA was mixed with wild-type CHO cells and seeded onto glass coverslips, fixed with ice-cold methanol, and stained with anti-HCNL1 antibodies, a monoclonal anti-HA antibody, and DAPI. For detection, fluorescently labeled secondary antibodies (Alexa488 or Cy3) were used. After mounting, cells were imaged under a confocal microscope. Zebrafish sperm were immobilized on adhesion microscope slides. Fixation, staining, and imaging were performed as for CHO cells. Additional information on immunocytochemical protocols is provided in *SI Appendix, Materials and Methods*.

Data Availability. Data generated and analyzed over the course of the current study are included within the paper or *SI Appendix*.

ACKNOWLEDGMENTS. We thank S. Wolf-Kümmeth and J. Goergen for technical support. This research was supported by the German Research Foundation (DFG, Grant BE5506/3-1 to T.K.B.).

1. B. Santoro *et al.*, Identification of a gene encoding a hyperpolarization-activated pacemaker channel of brain. *Cell* **93**, 717–729 (1998).
2. R. Gauss, R. Seifert, U. B. Kaupp, Molecular identification of a hyperpolarization-activated channel in sea urchin sperm. *Nature* **393**, 583–587 (1998).
3. A. Ludwig, X. Zong, M. Jeglitsch, F. Hofmann, M. Biel, A family of hyperpolarization-activated mammalian cation channels. *Nature* **393**, 587–591 (1998).
4. D. DiFrancesco, P. Tortora, Direct activation of cardiac pacemaker channels by intracellular cyclic AMP. *Nature* **351**, 145–147 (1991).
5. R. B. Robinson, S. A. Siegelbaum, Hyperpolarization-activated cation currents: From molecules to physiological function. *Annu. Rev. Physiol.* **65**, 453–480 (2003).
6. T. Berger, M. E. Larkum, H. R. Lüscher, High I(h) channel density in the distal apical dendrite of layer V pyramidal cells increases bidirectional attenuation of EPSPs. *J. Neurophysiol.* **85**, 855–868 (2001).
7. J. C. Magee, Dendritic Ih normalizes temporal summation in hippocampal CA1 neurons. *Nat. Neurosci.* **2**, 508–514 (1999).
8. G. L. Fain, F. N. Quandt, B. L. Bastian, H. M. Gerschenfeld, Contribution of a caesium-sensitive conductance increase to the rod photoresponse. *Nature* **272**, 466–469 (1978).
9. C. R. Bader, P. R. Macleish, E. A. Schwartz, A voltage-clamp study of the light response in solitary rods of the tiger salamander. *J. Physiol.* **296**, 1–26 (1979).
10. T. Strünker, L. Alvarez, U. B. Kaupp, At the physical limit—Chemosensation in sperm. *Curr. Opin. Neurobiol.* **34**, 110–116 (2015).
11. C. Trötschel *et al.*, Absolute proteomic quantification reveals design principles of sperm flagellar chemosensation. *EMBO J.* **39**, e102723 (2020).
12. S. Fechner *et al.*, A K(+)-selective CNG channel orchestrates Ca(2+) signalling in zebrafish sperm. *eLife* **4**, e07624 (2015).
13. A. Ludwig *et al.*, Two pacemaker channels from human heart with profoundly different activation kinetics. *EMBO J.* **18**, 2323–2329 (1999).
14. V. De-la-Rosa, E. Suárez-Delgado, G. E. Rangel-Yescas, L. D. Islas, Currents through Hv1 channels deplete protons in their vicinity. *J. Gen. Physiol.* **147**, 127–136 (2016).
15. I. S. Ramsey, M. M. Moran, J. A. Chong, D. E. Clapham, A voltage-gated proton-selective channel lacking the pore domain. *Nature* **440**, 1213–1216 (2006).
16. M. Sasaki, M. Takagi, Y. Okamura, A voltage sensor-domain protein is a voltage-gated proton channel. *Science* **312**, 589–592 (2006).
17. F. Tombola, M. H. Ulbrich, E. Y. Isacoff, The voltage-gated proton channel Hv1 has two pores, each controlled by one voltage sensor. *Neuron* **58**, 546–556 (2008).
18. B. Hille, *Ion Channels of Excitable Membranes*, (Sinauers Associates, Sunderland, MA, ed. 3, 2001).
19. Y. Jiang *et al.*, X-ray structure of a voltage-dependent K+ channel. *Nature* **423**, 33–41 (2003).
20. J. Payandeh, T. Scheuer, N. Zheng, W. A. Catterall, The crystal structure of a voltage-gated sodium channel. *Nature* **475**, 353–358 (2011).
21. T. Xue, E. Marbán, R. A. Li, Dominant-negative suppression of HCN1- and HCN2-encoded pacemaker currents by an engineered HCN1 construct: Insights into structure-function relationships and multimerization. *Circ. Res.* **90**, 1267–1273 (2002).
22. D. M. Starace, F. Bezanilla, A proton pore in a potassium channel voltage sensor reveals a focused electric field. *Nature* **427**, 548–553 (2004).
23. F. Tombola, M. M. Pathak, E. Y. Isacoff, Voltage-sensing arginines in a potassium channel permeate and occlude cation-selective pores. *Neuron* **45**, 379–388 (2005).
24. S. Sokolov, T. Scheuer, W. A. Catterall, Gating pore current in an inherited ion channelopathy. *Nature* **446**, 76–78 (2007).
25. K. Jurkat-Rott, J. Groome, F. Lehmann-Horn, Pathophysiological role of omega pore current in channelopathies. *Front. Pharmacol.* **3**, 112 (2012).
26. V. De La Rosa, I. S. Ramsey, Gating currents in the Hv1 proton channel. *Biophys. J.* **114**, 2844–2854 (2018).
27. E. M. Carmona *et al.*, Gating charge displacement in a monomeric voltage-gated proton (H_v1) channel. *Proc. Natl. Acad. Sci. U.S.A.* **115**, 9240–9245 (2018).
28. T. K. Berger, E. Y. Isacoff, The pore of the voltage-gated proton channel. *Neuron* **72**, 991–1000 (2011).
29. K. S. Shin, B. S. Rothberg, G. Yellen, Blocker state dependence and trapping in hyperpolarization-activated cation channels: Evidence for an intracellular activation gate. *J. Gen. Physiol.* **117**, 91–101 (2001).
30. L. Hong, M. M. Pathak, I. H. Kim, D. Ta, F. Tombola, Voltage-sensing domain of voltage-gated proton channel Hv1 shares mechanism of block with pore domains. *Neuron* **77**, 274–287 (2013).
31. L. Hong, I. H. Kim, F. Tombola, Molecular determinants of Hv1 proton channel inhibition by guanidine derivatives. *Proc. Natl. Acad. Sci. U.S.A.* **111**, 9971–9976 (2014).

Downloaded at DKFZ-HGF on November 13, 2020

32. X. Tao, A. Lee, W. Limapichat, D. A. Dougherty, R. MacKinnon, A gating charge transfer center in voltage sensors. *Science* **328**, 67–73 (2010).
33. F. Bezanilla, E. Perozo, D. M. Papazian, E. Stefani, Molecular basis of gating charge immobilization in Shaker potassium channels. *Science* **254**, 679–683 (1991).
34. C.-H. Lee, R. MacKinnon, Structures of the human HCN1 hyperpolarization-activated channel. *Cell* **168**, 111–120.e11 (2017).
35. S.-Y. Lee, J. A. Letts, R. MacKinnon, Dimeric subunit stoichiometry of the human voltage-dependent proton channel Hv1. *Proc. Natl. Acad. Sci. U.S.A.* **105**, 7692–7695 (2008).
36. H. P. Koch *et al*., Multimeric nature of voltage-gated proton channels. *Proc. Natl. Acad. Sci. U.S.A.* **105**, 9111–9116 (2008).
37. S. M. H. Alavi, J. Cosson, Sperm motility in fishes. (II) Effects of ions and osmolality: A review. *Cell Biol. Int.* **30**, 1–14 (2006).
38. Y.-H. Tu *et al*., An evolutionarily conserved gene family encodes proton-selective ion channels. *Science* **359**, 1047–1050 (2018).
39. I. V. Chizhmakov *et al*., Selective proton permeability and pH regulation of the influenza virus M2 channel expressed in mouse erythroleukaemia cells. *J. Physiol.* **494**, 329–336 (1996).
40. K. Shimbo, D. L. Brassard, R. A. Lamb, L. H. Pinto, Ion selectivity and activation of the M2 ion channel of influenza virus. *Biophys. J.* **70**, 1335–1346 (1996).
41. F. V. Campos, B. Chanda, B. Roux, F. Bezanilla, Two atomic constraints unambiguously position the S4 segment relative to S1 and S2 segments in the closed state of Shaker K channel. *Proc. Natl. Acad. Sci. U.S.A.* **104**, 7904–7909 (2007).
42. A. Chamberlin *et al*., Hydrophobic plug functions as a gate in voltage-gated proton channels. *Proc. Natl. Acad. Sci. U.S.A.* **111**, E273–E282 (2014).
43. H. Shen *et al*., Structure of a eukaryotic voltage-gated sodium channel at near-atomic resolution. *Science* **355**, eaal4326 (2017).
44. A. L. Bennett, I. S. Ramsey, CrossTalk opposing view: Proton transfer in Hv1 utilizes a water wire, and does not require transient protonation of a conserved aspartate in the S1 transmembrane helix. *J. Physiol.* **595**, 6797–6799 (2017).
45. T. E. DeCoursey, CrossTalk proposal: Proton permeation through H_V 1 requires transient protonation of a conserved aspartate in the S1 transmembrane helix. *J. Physiol.* **595**, 6793–6795 (2017).
46. T. E. DeCoursey, Voltage-gated proton channels. *Cell. Mol. Life Sci.* **65**, 2554–2573 (2008).
47. S. L. Marguet *et al*., Treatment during a vulnerable developmental period rescues a genetic epilepsy. *Nat. Med.* **21**, 1436–1444 (2015).
48. A. K. Schlusche, "The role of HCN channels in the prenatal development of the cerebral cortex in the mouse (Mus musculus, Linnaeus 1758)," PhD thesis, University of Cologne, Cologne, Germany (2017).
49. T. Erickson, T. Nicolson, Identification of sensory hair-cell transcripts by thiouracil-tagging in zebrafish. *BMC Genomics* **16**, 842 (2015).
50. U. B. Kaupp, T. Strünker, Signaling in sperm: More different than similar. *Trends Cell Biol.* **27**, 101–109 (2017).
51. X. Cai, X. Wang, D. E. Clapham, Early evolution of the eukaryotic Ca2+ signaling machinery: Conservation of the CatSper channel complex. *Mol. Biol. Evol.* **31**, 2735–2740 (2014).
52. T. Strünker *et al*., A K+-selective cGMP-gated ion channel controls chemosensation of sperm. *Nat. Cell Biol.* **8**, 1149–1154 (2006).
53. R. Seifert *et al*., The CatSper channel controls chemosensation in sea urchin sperm. *EMBO J.* **34**, 379–392 (2015).

Downloaded at DKFZ-HGF on November 13, 2020